Analysis of two SMC H II Regions Considering Thermal Inhomogeneities: Implications for the Determinations of Extragalactic Chemical Abundances [1]

María A. Peña-Guerrero[2]

guerrero@astroscu.unam.mx

Antonio Peimbert[2]

antonio@astroscu.unam.mx

Manuel Peimbert[2]

peimbert@astroscu.unam.mx

and

María Teresa Ruiz[3]

mtruiz@das.uchile.cl

ABSTRACT

We present long slit spectrophotometry considering the presence of thermal inhomogeneities (t^2) of two H II regions in the Small Magellanic Cloud (SMC): NGC 456 and NGC 460. Physical conditions and chemical abundances were determined for three positions in NGC 456 and one position in NGC 460, first under the assumption of uniform temperature and then allowing for the possibility of thermal inhomogeneities. We determined t^2 values based on three different methods: i) by comparing the temperature derived using oxygen forbidden lines with the temperature derived using helium recombination lines, ii) by comparing the abundances derived from oxygen forbidden lines with those derived from

[2]Instituto de Astronomía, Universidad Nacional Autónoma de México, Apdo. Postal 70-264, México 04510 D.F., México

[3]Departamento de Astronomía, Universidad de Chile, Casilla Postal 36D, Santiago de Chile, Chile

oxygen recombination lines, and iii) by comparing the abundances derived from ultraviolet carbon forbidden lines with those derived from optical carbon recombination lines. The first two methods averaged $t^2=0.067 \pm 0.013$ for NGC 456 and $t^2=0.036 \pm 0.027$ for NGC 460. These values of t^2 imply that when gaseous abundances are determined with collisionally excited lines they are underestimated by a factor of nearly 2. From these objects and others in the literature, we find that in order to account for thermal inhomogeneities and dust depletion, the O/H ratio in low metallicity H II regions should be corrected by 0.25 - 0.45 dex depending on the thermal structure of the nebula, or by 0.35 dex if such information is not available.

Subject headings: H II regions: abundances—galaxies: H II regions – H II regions: thermal inhomogeneities — H II regions: individual (NGC 456, NGC 460)

1. Introduction

The Magellanic Clouds play a fundamental role in astrophysics because they are the closest laboratory we have to probe the extragalactic distance scale and the theories about chemical evolution of stars and galaxies. They are close enough to be able to identify individual objects and isolate them from their environment. In the case of chemical abundance studies of H II regions, it is possible to perform observations that avoid bright stars, Wolf-Rayet stars, and supernova remnants; this can translate in extremely good equivalent widths in emission, $\mathrm{EW}_{em}(\mathrm{H}\beta) \gtrsim 250$ Å.

There have been many studies of the chemical composition of H II regions in the Magellanic Clouds (e.g. Peimbert & Torres-Peimbert 1976; Pagel et al. 1978; Westerlund 1990; Caplan et al. 1996; Peimbert et al. 2000). It has been found that the chemical composition within each cloud is uniform, and that the SMC has lower metallicity (approximately 0.40 dex) than the Large Magellanic Cloud (LMC); making the SMC the best object to study low metallicity environments. In particular, H II regions of the SMC provide the means to study low metallicity star-forming neighborhoods and NGC 456 is one of the brightest H II regions of the SMC (Peimbert & Torres-Peimbert 1976). In this study the number of lines presented for NGC 456 and NGC 460 is considerably larger than in previous works.

Almost all studies of H II regions use the direct method to determine gaseous abundances, and implicitly assume that this value represents the chemical abundances of the ISM. The direct method uses collisionally excited lines (CELs) to obtain chemical abundances, and presuppose a homogeneous temperature structure. When abundances are calculated us-

ing recombination lines (RLs), they are approximately factors of 2 higher than abundances obtained with CELs; this is now known as the abundance discrepancy factor (ADF) problem. Moreover, the depletion into dust grains can account for a large fraction of the oxygen atoms.

Esteban et al. (1998) measured the depletion into dust in the Orion nebula and suggested that a 0.08 dex correction to the O/H ratio should be included when considering H II regions. More recent studies of the Orion nebula suggest that the correction is higher (Mesa-Delgado et al. 2009b; Simón-Díaz & Stasińska 2011) while recent studies of depletion of Mg, Si, and Fe suggest that the correction depends on the O/H ratio of the specific H II region (Peimbert & Peimbert 2010), reaching a fraction of up to 28% for high metallicity regions.

Peimbert (1967) proposed to take into account t^2 when using CELs to determine abundances in modeling H II regions, and found that spatial thermal fluctuations of approximately 20% are capable of producing errors of factors of 2 to 3 on the determination of chemical abundances. The additional complications to calculate abundances using t^2, along with the fact that there is no tailored physical model to fit temperature inhomogeneities, have made its reception within the community poor.

Since the idea of Peimbert's temperature inhomogeneities was introduced, several explanations about where such temperature inhomogeneities could be coming from have been proposed: shock waves, shadowed regions, advancing ionization fronts, multiple ionizing sources, X-rays, magnetic reconnection, and inhomogeneous chemical composition, among others (e.g. Peimbert & Peimbert 2006; Tsamis & Péquignot 2005, and references therein). However, most of these explanations are capable of either producing only a fraction the t^2 value found in observations or, under fine-tuned circumstances, the total observed t^2 values.

For most objects, two explanations are capable of producing the observed t^2 values: a) the observed t^2 values come from a variety of mechanisms in a chemically homogeneous medium, where each mechanism is only responsible for a fraction of the total; and b) the presence of chemical inhomogeneities within the photoionized region. As of now, no complete self-consistent model has been proposed for either explanation: models for explanation (a) have not been able to explain where all the required energy to keep these thermal inhomogeneities comes from, while models for explanation (b) have not been able to describe the exact characteristics and evolution of the proposed high metallicity inclusions. As for abundance determinations: option (a) would indicate that RLs give the correct abundances, or that one could use CELs and the formalism of t^2 of Peimbert & Costero (1969) to determine abundances; and models of option (b) imply that the chemical abundance is intermediate

between those obtained from CELs adopting t^2=0.00, and RLs adopting a chemically inhomogeneous medium (Tsamis & Péquignot 2005). For either option, the abundances determined using CELs with t^2=0.00 need a systematic correction.

Additional evidence supporting chemically homogeneous models with large t^2 values implied by the ADF problem comes from: the theoretical vs. observational $\Delta Y/\Delta O$ ratio, abundances of F and G young stars of the solar vicinity vs. abundances of H II regions, oxygen abundances of O and B stars vs. abundances of H II regions, protosolar abundances vs. H II region abundances, considering the effect of Galactic chemical evolution (see Peimbert & Peimbert 2011, and references therein).

In Sections 2 and 3 the observations and reduction procedure are described. In Section 4 temperatures and densities are derived from four and three different line intensity ratios, respectively; also in this section we derive the mean square temperature inhomogeneities, t^2, in three different ways: i) from the comparison of the abundances of O II lines to those of [O III] lines, ii) using He I lines, and iii) from the comparison of the abundance of C II lines to those of [C III] λ 1907 + C III] λ 1909 lines. In Section 5 we determine ionic abundances with three different methods: i) based on RLs, ii) based on CELs, and iii) correcting CELs for t^2; while the total abundances derived from these methods are presented in Section 6. In Section 7 we present the direct method and its shortcomings, the typical correction to the O/H ratio for low metallicity H II regions, and the implications for the determinations of extragalactic chemical abundances. Finally, the discussion and conclusions are presented in Sections 8 and 9, respectively.

2. Observations

The observations were obtained during the night of September 10$^{\text{th}}$ of 2002 with the Focal Reducer Low Dispersion Spectrograph 1, FORS1, at the Very Large Telescope, VLT, Melipal in Cerro Paranal, Chile. We used three grism settings: GRIS-600B+12, GRIS-600R+14 with filter GG435, and GRIS-300V with filter GG375 (see Table 1).

The slit was oriented almost east-west (position angle 82.5º) to observe the brightest regions of NGC 456 (α=1^{h}13^{m}50.8^s, δ=-73º18'03.2") which we called NGC 456 Position 2. The linear atmospheric dispersion corrector, LACD, was used to keep the same observed region within the slit regardless of the air mass value. The slit length was 410" and the slit width was set to 0.51", this setting was chosen to have the resolution to deblend the [O II] line λ 3726 from λ 3729 when using the GRIS-600B+12. Three observations were made with each grism configuration to be able to identify and remove cosmic rays.

The aperture extractions were made for a length of 5.6" for NGC 456 Position 2; NGC 456 Position 1 is centered 11.4" east of Position 2 and has a length of 17.2", and NGC 456 Position 3 is centered 19.4" west of Position 2 and has a length of 22.4" (note there is a 3.2" gap to avoid a bright star between positions 2 and 3, see Figure 1). The eastern part of the slit passed through the outer parts of NGC 460; we defined NGC 460 Position 1 as the region centered 199" east of NGC 456 Position 2, with a length of 40".

The spectra were reduced using IRAF[1] reduction packages, following the standard procedure of bias subtraction, aperture extraction, flat fielding, wavelength calibration and flux calibration. For flux calibration the standard stars LTT 2415, LTT 7389, LTT 7987 and EG 21 were used (Hamuy et al. 1992, 1994). The observed spectra are presented in Figure 2; a zoom-in of the region around $\lambda 4600$ of the spectrum of NGC 456-2 is presented in Figure 3 to show the quality of the data.

3. Line Intensities and reddening correction

The procedure of line measurement was done using the `splot` task of the IRAF package. Line intensities were measured by integrating the flux in the line between two limits over the local continuum estimated by eye. There were a few cases where line blending was found. In this situation we used a multiple Gaussian profile procedure. The error in the flux calibration has been estimated to be 1%; the contribution to the errors due to the noise was estimated from the continuum. The final adopted errors were estimated using standard error procedures.

The reddening correction, $C(\mathrm{H}\beta)$, and the underlying absorption, $EW_{abs}(\mathrm{H}\beta)$, were fitted simultaneously to the theoretical ratios. We adopted the extinction law of Seaton (1979), and the underlying absorption ratios obtained from the work by González-Delgado et al. (1999) and from the theoretical ratios determined with the program `INTRAT` by Storey & Hummer (1995).

The Balmer and helium emission lines were corrected for underlying absorption, and the equivalent widths in absorption adopted are presented in Table 2. The extinction law values used are presented in Tables 3 and 4. The physical conditions used for `INTRAT` were T_e=10,000 K and n_e=100 cm^{-3}, this is only a first guess, but since the hydrogen lines are nearly independent from temperature and density no further corrections were necessary.

The emission line intensities of all positions in NGC 456 and NGC 460 are presented in

---

[1]IRAF is distributed by NOAO, which is operated by AURA, under cooperative agreement with NSF.

Tables 3 and 4, respectively. Table 3, column (1) presents the adopted laboratory wavelength, λ, column (2) the identification for each line, column (3) presents the extinction law value used for each line (Seaton 1979), $f(\lambda)$. Columns (4-6) present the data from NGC 456-1, showing: the observed flux relative to Hβ, $F(\lambda)$; the flux corrected for reddening relative to Hβ, $I(\lambda)$; and the percentage error associated with those intensities, respectively. Columns (7-9) and (10-12) present the same data as columns (4-6) but for positions 2 and 3, respectively. In Table 4 the columns are the same as the first 6 columns of Table 3 but for Position 1 of NGC 460. The EW_{abs}(Hβ), C(Hβ), EW(Hβ), as well as the F(Hβ) and $I(\beta)$ for each position in both objects are also presented in these tables.

4. Physical Conditions

4.1. Temperatures and densities

The sources for the atomic data of CELs in the used IRAF are presented in Table 5 – for studies of nebulae with higher densities, we recommend to use more recent O^+ collisional strengths such as those from Wang et al. (2004); Montenegro et al. (2006); Pradhan et al. (2006), and Tayal (2007). The temperatures and densities in Table 6 were determined using the line intensities presented in Tables 3 and 4. These determinations were done with the `temden` task in IRAF, which models populations in five-, six-, or eight-level ions to derive the physical conditions.

4.2. Temperature Inhomogeneities

Instead of assuming a homogeneous temperature throughout the objects we took into account inhomogeneities in the temperature structure, which are described by the formalism developed by Peimbert (1967). To derive the ionic abundance ratios we used the average temperature, T_0, and the mean square temperature inhomogeneities, t^2, defined as follows:

$$T_0(ion) = \frac{\int T_e(\mathbf{r})N_e(\mathbf{r})N_{ion}(\mathbf{r})dV}{\int N_e(\mathbf{r})N_{ion}(\mathbf{r})dV}, \tag{1}$$

$$t^2(ion) \equiv \frac{\int (T_e - T_0)^2 N_e(\mathbf{r})N_{ion}(\mathbf{r})dV}{T_0^2 \int N_e(\mathbf{r})N_{ion}(\mathbf{r})dV}, \tag{2}$$

where N_e and N_{ion} are the electron and the ion densities, respectively, of the line of sight, and V is the observed volume.

Two independent temperatures are required to infer T_0 and t^2: one that weights preferentially the high-temperature regions and another that weights preferentially the low-temperature regions (Peimbert 1967). The temperatures that weight preferentially the high temperature region were defined as in Peimbert et al. (2002):

$$T_{4363/5007} = T_0 \left[\left(1 + \frac{t^2}{2} \left(\frac{91300}{T_0} - 3 \right) \right) \right], \tag{3}$$

for the O^{++} region; for the O^+ region we used a similar equation for the [O II] $\lambda\lambda$ 3727 and 7325 lines with an energy corresponding to 97800 K.

Following the literature (Peimbert 2003; Peimbert et al. 2005, and references therein), we can determine a t^2 value from the helium lines. The HELIO10 program determines a a temperature that weights preferentially the low temperature regions from the He I lines. This temperature can be determined with the HELIO10 program, which uses an analysis involving a maximum likelihood method (see Section 5.1), which finds the best simultaneous fit to T(He I), n_e, τ_{3889}, and He^+/H^+. This T(He I) can be combined with the temperatures derived from the oxygen CELs to derive t^2 and T_0. In positions 1 and 3 of NGC 456, we simply adopted the t^2 value obtained from the He I lines: $t^2=0.035\pm0.032$ and $t^2=0.040\pm0.040$, respectively. For NGC 456-2 and NGC 460-1 the values we obtained with the HELIO10 program are $t^2=0.053\pm0.017$ and $t^2=0.032\pm0.032$, respectively.

We used the temperature derived from the ratio of the multiplet 1 of O II lines to the CELs of [O III] as given by equations [8]−[12] in the work of (Peimbert et al. 2005),

$$T_{(\text{OII}/[\text{OIII}])} = T_{4651/5007} = f_1(T_0, t^2). \tag{4}$$

With the oxygen RLs in NGC 456-2 we obtained that T_0 =10,120 K and $t^2=0.083\pm0.019$ using the equations above. For the case of NGC 460-1, $T_0=11,370$ K and $t^2=0.041\pm0.027$ also with oxygen RLs. In NGC 456 - 2 the oxygen is about 80% twice ionized (see Section 5.3), hence the value of $t^2(\text{He}^+) \approx t^2(\text{O}^{++})$. NGC 460 has approximately 60% of its oxygen twice ionized, but since we only have one other t^2 determination to compare it with, we will also assume that $t^2(\text{He}^+) \approx t^2(\text{O}^{++})$.

The combined values of thermal inhomogeneities from the HELIO10 program and from the oxygen RLs resulted in $t^2=0.067\pm0.013$ for NGC 456 Position 2 and $t^2=0.036\pm0.027$ for NGC 460 Position 1.

We were able to obtain the C^{++} ionic abundance from both UV CELs and from optical RLs (see Section 5). We found that the abundances are not consistent with a homogeneous temperature structure. A possible value for $t^2(\text{C}^{++})$ in NGC 456 is 0.08$\pm$0.04; this value represents the t^2 of the UV observed region.

The t^2 determinations in this paper, with the exception of NGC 456-2, lie within typical values of thermal inhomogeneities measured for Galactic H II regions which range between 0.03 and 0.04 (García-Rojas & Esteban 2007). The t^2 determination of NGC 456 Position 2 lies within typical values for extragalactic H II regions, which range between 0.03 and 0.11. This is probably because in regions that are farther away it is impossible to isolate "simple" volumes and one observes the sum of many physical processes: shadows, high density knots, shock waves, ionization fronts, photoionization, etc.

5. Ionic Abundances

5.1. Helium

We used the HELIO10 program to obtain the ionic abundance of He$^+$, presented in Table 7. This program is described in Peimbert et al. (2011) and it uses a maximum likelihood method to search for the set of parameters (T_0, t^2, n_e, τ_{3889}, T(He I), and He$^+$/H$^+$) that produce the optimal simultaneous fit to all the observed helium lines as well as the measured T_e[O III] and T_e[O II]. The effective recombination coefficients for the H I and He I used were those given by Storey & Hummer (1995) for H and by Benjamin et al. (1999) and Porter et al. (2007) for He. The collisional contribution was estimated from Sawey & Berrington (1993) and Kingdon & Ferland (1995). The optical depth effects in the triplets were estimated with calculations made by Benjamin et al. (2002).

Correction for underlying stellar absorption is also important for helium lines, in a similar way as is for hydrogen lines. Hence, to correct for underlying He I absorption for lines with $\lambda <5000$ Å we used values determined by González-Delgado et al. (1999), and for redder lines we used the same values as in Peimbert et al. (2005).

Between 9 and 12 He I lines were used as input in the HELIO10 program to determine the t^2 value for each observed position in both NGC 456 and NGC 460.

The t^2 derived from He I lines can be used to redetermine abundances in the high-temperature regions considering temperature inhomogeneities, due to the similar ionization potentials of He$^+$ and O^{++}. Since the He II line λ 4686 was not detected, the fraction of He^{++}/He$^+$ is smaller than 1×10^{-3} for NGC 456 Position 1, 4×10^{-4} for NGC 456 Position 2, and 3×10^{-3} for NGC 456 Position 3 and NGC 460 Position 1.

5.2. C and O from Recombination Lines

The ionic abundance for C^{++} presented in Table 7, was obtained from the measurement of the λ 4267 line of C II. The effective recombination coefficient used was that determined by Davey et al. (2000) for Case A and with T =10,000 K. Although we did measure the λ 4267 line in positions 1 and 3 of NGC 456 and in Position 1 of NGC 460, the errors were too large to provide any information other than an upper limit.

The effective recombination coefficients for determining the ionic abundance of oxygen from the lines of the multiplet 1 of O II were taken from Peimbert et al. (1993) and Storey (1994) assuming Case B for T_e =10,000 K and N_e =100 cm^{-3}. The multiplet consists of eight lines each of which depends on the electron density even though the sum of their intensities, I(sum), does not (Ruiz et al. 2003; Bastin & Storey 2006; Peimbert & Peimbert 2010). Since these lines are very faint, it is often necessary to estimate the unobserved and/or blended lines.

The measurements of the O II lines in NGC 456-2 and NGC 460-1 are presented in Tables 3 and 4; the abundances derived from these lines are also presented in Table 7. The errors in the measurements of the oxygen RLs in positions 1 and 3 of NGC 456 were too large to provide useful information. For the first two mentioned cases, we were able to detect four of the eight lines in the multiplet. Due to the spectral resolution of the observations, those lines were blended into two pairs: $\lambda\lambda$4639+42 and $\lambda\lambda$4649+51.

Measurements of RLs of heavy elements are not common in long-slit spectrophotometry. Contamination from blends of other lines of other ions could be a concern. To check this, we looked into echelle observations of H II regions with good S/N (Peimbert 2003; Esteban et al. 2004; García-Rojas et al. 2004; García-Rojas & Esteban 2007); the only other lines that appear in this region of the spectra are: N III $\lambda\lambda$ 4641 and N II λ 4643. The contribution of the sum of these two N lines compared to the sum of the four O lines observed is about 10% for objects with metallicity and N/O close to solar, and less than 4% for 30 Doradus that has N/O about three times less than solar and slightly higher than the SMC; given our S/N, we will ignore it (see Figure 3).

5.3. Ionic Abundances from Collisionally Excited Lines

The ionic carbon abundance from CELs was determined with UV spectra of NGC 456 obtained from the on-line data presented by Bonatto et al. (1995). We measured the [C III] λ1907 C III]λ1909 lines using the O III] $\lambda\lambda$1660+66 lines with the UV C(Hβ) presented in Seaton (1979), and the atomic data contained in the task `ionic` of IRAF v2.15.1. The

value of the C^{++}/H^+ abundance is presented in Table 8 with and without considering thermal inhomogeneities.

With the exception of carbon, all other ionic abundances presented in Table 8 were determined using the task `abund` of IRAF considering only the low and medium-ionization zones, which correspond to the low and high-ionization zones of the present work. For positions 1, 2, and 3 of NGC 456 we used T_{low} =13,500 K, 12,400 K, and 12,600 K, respectively; and T_{high} = 12,650 K, 12,165 K, and 12,300 K, respectively.

Ionic abundances considering thermal inhomogeneities, $t^2 \neq 0.000$, were obtained using the traditional determinations, $t^2 = 0.000$, corrected by the formalism presented by Peimbert & Costero (1969), see also Peimbert et al. (2004).

6. Total Abundances

In general we observed that all positions in NGC 456 presented a high O ionization degree implying that there is no substantial amount of He^0. The amount of He^+ is similar in all positions of both NGC 456 and NGC 460, which may indicate that the ionization degree is also similar in Position 1 of NGC 460.

In the case of C and N, total gaseous abundances were determined with the following equations:

$$\frac{N(C)}{N(H)} = \text{ICF}(C)\frac{N(C^{++})}{N(H^+)} \tag{5}$$

and

$$\frac{N(N)}{N(H)} = \text{ICF}(N)\frac{N(N^+)}{N(H^+)}, \tag{6}$$

where we used the ionization correction factor (ICF) for C with respect to O of Garnett et al. (1995), and multiplied it by the fraction of C^{++}/O^{++} in NGC 456-2 following Peimbert (2003); this value amounted to 1.27. The N total gaseous abundance was determined adopting the predicted ICF(N) of Peimbert & Costero (1969), $N(O)/N(O^+)$.

The total gaseous abundances for Cl, S, and Ar were determined with the following equations:

$$\frac{N(Cl)}{N(H)} = \text{ICF}(Cl)\frac{N(Cl^{++})}{N(H^+)}, \tag{7}$$

$$\frac{N(S)}{N(H)} = \text{ICF}(S)\frac{N(S^+) + N(S^{++})}{N(H^+)}, \tag{8}$$

and

$$\frac{N(\text{Ar})}{N(\text{H})} = \text{ICF}(\text{Ar})\frac{N(\text{Ar}^{++}) + N(\text{Ar}^{+++})}{N(\text{H}^+)}; \qquad (9)$$

where the corresponding ICFs were estimated from Garnett (1989) for Cl, in the case of S from Peimbert et al. (2005), and for Ar the ICF was taken from Liu et al. (2000). For NGC 456-2 these values amounted to 1.26, 1.36, and 1.30, respectively; and 1.26, 1.12, and 1.71 for NGC 460-1.

Following Peimbert & Costero (1969), total gaseous abundances of O and Ne were calculated with the equations:

$$\frac{N(\text{O})}{N(\text{H})} = \frac{N(\text{O}^+) + N(\text{O}^{++})}{N(\text{H}^+)} \qquad (10)$$

and

$$\frac{N(\text{Ne})}{N(\text{H})} = \frac{N(\text{O}^+) + N(\text{O}^{++})}{N(\text{O}^{++})} \times \frac{N(\text{Ne}^{++})}{N(\text{H}^+)}. \qquad (11)$$

Total gaseous abundances for all available elements are presented in Tables 9 and 10 for NGC 456 positions 1, 2, and 3, and in Table 11 for NGC 460 Position 1. All these abundances are corrected by depletion of O in dust according to Peimbert & Peimbert (2010). Within the errors, abundances in all three positions of NGC 456 are very similar. Observations with higher S/N of NGC 456-1, -3 and of NGC 460-1 would allow to measure a more accurate value of t^2.

According to Peimbert & Peimbert (2010), a correction of 0.10 dex should be made to the total O abundances due to depletion of oxygen in dust. The adopted total abundance values for all available elements are presented in Tables 12 and 13. For comparison, we also present protosolar abundances and abundances of the Orion nebula, NGC 6822, and NGC 346, which is the brightest H II region of the SMC (Peimbert et al. 2000). In addition to this, we obtained an abundance determination for the ISM of the solar vicinity from the Galactic gradient derived from H II regions, that amounted to $12+\log(\text{O/H}) = 8.81$ once corrected by 0.12 for dust depletion (Esteban et al. 2005).

7. A Systematic Correction to the Direct Method

7.1. The Direct Method and its Shortcomings

The ADF is defined as the ratio of abundances determined using RLs vs. abundances obtained with CELs. ADFs are now well established for both Planetary Nebulae

and H II regions. RLs have a temperature dependence given approximately by $I \propto T_e^{-1}$, thus are brighter at lower temperatures; whereas CELs have a much stronger dependence, $I \propto exp(\mathrm{k}T_e/\Delta E)T_e^{-1/2}$, and thus brighter at higher temperatures.

Several studies (Peimbert et al. 1993, 1995; Tsamis et al. 2003, 2004; Peimbert et al. 2005; García-Rojas & Esteban 2007; Peimbert et al. 2007; Esteban et al. 2009, and references therein) have shown that ADF typical values are from 1.5 to 3 for most H II regions, and from 1.5 to 5 for most Planetary Nebulae. This is clear evidence that the traditional or direct method of abundance determinations – involving the assumption of homogeneous temperature determined from the emission line ratio 4363/(4959+5007) Å of [O III] – needs to be corrected. Since the work of Peimbert (1967) and Peimbert & Costero (1969), temperature inhomogeneities have been presented as a viable solution to the so called ADF problem. Peimbert & Peimbert (2011) discuss several methods that have been used to obtain t^2 values based on: i) the comparison between the temperatures derived from the ratio of the Balmer and Paschen continua to the Balmer line intensities and the temperatures derived from CELs; ii) the comparison of the C^{++} abundances derived using [C III]+C III] with abundances obtained from C II; iii) the comparison of O^{++} abundances derived with [O III] with abundances obtained using O II; iv) the comparison of the temperature that can be derived from He I lines to the temperatures derived from CELs; v) a high spatial resolution map of 1.5×10^6 columnar temperatures in the Orion nebula determined by O'Dell et al. (2003); and vi) the comparison of the different ways to calibrate Pagel's method. In all cases, the t^2 values are consistent with each other and the ADF problem goes away.

In the case of photoionization models, the intensity of nebular lines (such as λ 3727 [O II], or λ 6584 [N II]) can be adjusted in most models of both Planetary Nebulae and H II regions; however, auroral lines (such as λ 4363 [O III]) are in general not adjusted in those photoionization models.

7.2.   Typical Correction for Low Metallicity H II regions

We find that O/H abundances in H II regions determined with the direct method are underestimated and have to be corrected by factors of 0.25 - 0.45 dex. The correction we propose is due to two distinct and important physical processes: thermal inhomogeneities and depletion of oxygen into dust grains.

When allowing thermal inhomogeneities to exist in the abundance determination process, we find that the derived oxygen abundances in H II regions increase by 0.15 - 0.35 dex, depending on the particular characteristics of the thermal structure of each photoionized

region.

According to Peimbert & Peimbert (2010), abundances of photoionized regions require a correction of 0.09 - 0.10 dex for low metallicity H II regions due to depletion of oxygen into dust. Therefore the total correction amounts to about 0.35 dex in the total O abundance.

Many objects have t^2 determined with uncertainties larger than about 0.030, and frequently these determinations are consistent with t^2=0.000; the fact that many such objects exist does not mean that the t^2=0.000 or that there are many objects with negligible temperature inhomogeneities. Since all the objects where the determinations have uncertainties smaller than 0.015, are not consistent with a homogeneous temperature, it means that most objects have meaningful temperature inhomogeneities. To ignore the presence of these inhomogeneities because the data quality is not good enough, produces a very large bias in the study of H II regions in general. For this reasons we recommend to use this average correction of 0.35 dex in the total O abundance, and to explicitly present it so that, if the recommended correction improves with time, it is clear what to do.

7.3. Implications for the Determinations of Extragalactic Chemical Abundances

Studies of abundances in H II regions can also be used to check our understanding of the chemical evolution of our own Galaxy. Peimbert & Peimbert (2011) and Carigi & Peimbert (2011) find that careful determination of chemical abundances in H II regions (once corrected for depletion of oxygen into dust and for temperature inhomogeneities), are consistent with: i) the protosolar abundances after correcting them for the Galactic chemical evolution (Asplund et al. 2009; Carigi & Peimbert 2011), ii) young F and G stars of the solar vicinity (Bensby & Feltzing 2006), and iii) O and B stars of the Orion region (Przybilla et al. 2008; Simón-Díaz & Stasińska 2011).

Since the afore mentioned methods of determining abundances for stars and H II regions are entirely independent, the consistency in the results allows to individually validate each method. In particular it implies that a model with temperature inhomogeneities is a better approximation to reality than the direct method, that considers a homogeneous temperature structure.

Almost all studies of H II regions in the literature are made assuming homogeneous, or nearly homogeneous, temperature throughout the whole object, hence, the abundances derived from these works are underestimated by a factor of approximately 2. The study of abundances in low metallicity H II regions is important to set limits in the models of various areas

of astrophysics such as the radial abundance gradients in spiral galaxies (Vila-Costas & Edmunds 1992; Zaritsky et al. 1994; Esteban et al. 2005), the chemical evolution of starburst galaxies (e.g. Liu et al. 2008; Pérez-Montero et al. 2008; Bordalo & Telles 2011; Carigi & Peimbert 2011; Peimbert & Peimbert 2011), the mass-luminosity relation and the mass-metallicity relation (e.g. Tremonti et al. 2004; Kewley & Ellison 2008; Mannucci et al. 2010; Thuan et al. 2010), the initial mass function, star formation rate and yield determinations (e.g. Carigi et al. 2006; Pilyugin et al. 2007; Peimbert & Peimbert 2011), and the primordial helium abundance (Peimbert et al. 2007; Izotov 2010; Peimbert et al. 2010, and references therein), among others. Consequently, it is of great importance for these studies not to use abundances derived from the direct method, and to use abundances obtained with a method that either allows the presence of thermal inhomogeneities or is not affected by them (e.g. CELs corrected by temperature inhomogeneities or RLs).

8.   Discussion: the Thermal Structure of Gaseous Nebulae

In photoionization models, the temperature is nearly homogeneous because the processes considered for both heating and cooling are nearly proportional to the density squared. Strong thermal inhomogeneities require processes that generate either heating or cooling that are not proportional to the density squared.

Observationally, the ADF problem emerges when a homogeneous temperature is assumed. O'Dell et al. (2003) presented a high spatial resolution map of the columnar electron temperatures of the Trapezium with which they found a t^2 value from different lines of sight within the nebula, whereas Tsamis & Walsh (2011), studying components and different velocities, found that each line of sight has thermal inhomogeneities.

All available explanations in the literature for the presence of the ADF require the presence of thermal inhomogeneities. There are two families of mechanisms that produce temperature inhomogeneities: i) an inhomogeneous cooling function of the photoionized region, i.e. chemical inhomogeneities (Torres-Peimbert et al. 1990; Tenorio-Tagle 1996; Liu et al. 2000; Tsamis & Péquignot 2005; Ercolano et al. 2007; Stasińska et al. 2007), and ii) an inhomogeneous heating, e.g. shock waves, advancing photoionization fronts, shadowed regions, magnetic reconnection (Peimbert & Peimbert 2006, and references therein). There is a small fraction of Planetary Nebulae and H II regions that are chemically inhomogeneous; these objects will not be discussed in this paper. Models that are chemically inhomogeneous predict abundances that are intermediate between those derived with the direct method and from RLs. For most objects an inhomogeneous heating mechanism is in better agreement with abundances derived from stellar objects (see section 7.3), and with the thermal structure of

the Orion nebula (see section 7.1). Moreover, t^2 values derived with independent methods are consistent with each other within the errors. Specifically, the fact that the t^2 values from He and O are consistent, implies that the material in the nebulae is well mixed since these elements have different formation histories (Carigi & Peimbert 2011).

Typical photoionization model values of t^2 are about one order of magnitude smaller than the temperature inhomogeneities determined from observations. With near photoionized objects such as the Orion nebula, extremely detailed studies can be made to measure precise values of t^2: e.g. O'Dell et al. (2003) presented a high spatial resolution map of the columnar electron temperatures of the Trapezium with which they found that shadowed regions can significantly contribute to the observed thermal inhomogeneities; Tsamis & Walsh (2011) and Tsamis et al. (2011) were able to isolate individual high density regions and found that CELs underestimate abundances; and Mesa-Delgado et al. (2009a) and Mesa-Delgado et al. (2009b) studied the head of HH 202 and found that the ionization front has a t^2 value significantly higher than that of the nebula.

Photoionization models include an energy injection proportional to the density squared; this should be a good approximation if the energy were dominated by photoionization. However, the measurements of the filling factor (which is defined as the occupied volume over the total volume) argue against such an energy budget model. Typical filling factor values for H II regions are in the 0.01-0.10 range. These values are showing that H II regions are pretty much empty, but they are not showing the origin of the energy that is keeping the material apart. This is strong evidence that the traditional energy budget model to study H II regions is incomplete. The fact that it is not known what is feeding the filling factor in H II regions does not mean that abundance results considering $t^2>0.00$ are incorrect, it means that models have to be improved to better understand the physics and astrophysics of these objects. Temperature inhomogeneities are showing that photoionization models have to be corrected to account for the additional physics that has not been included.

Chemical abundances determined using CELs strongly depend on the thermal structure of the nebula, whereas abundances obtained with RLs do not. Even though we know many processes capable of generating temperature inhomogeneities, we do not know, quantitatively, the relative importance of each one of them. We can estimate the magnitude and the effect that these thermal inhomogeneities have on the chemical abundances. Although it is interesting to study the origin of such thermal inhomogeneities, it is beyond the scope of this paper to do so. In order to determine abundances we need to know the value of t^2 and not what is producing it.

9. Conclusions

A detailed analysis was performed for the SMC H II regions NGC 456 and NGC 460. This analysis involves abundance determinations considering thermal inhomogeneities ($t^2 \neq 0.00$); for the purpose of comparison with other authors, we also determined abundances with the direct or traditional method, which assumes a homogeneous temperature structure ($t^2 = 0.00$). The abundances of NGC 346 (Peimbert et al. 2000), NGC 456, and NGC 460, are similar once corrected for dust depletion. The O/H abundances of the SMC H II regions are 0.58 dex lower than those of the ISM of the solar vicinity, and 0.46 dex lower than the solar photosphere. This indicates that the Small Magellanic Cloud is chemically less evolved than the Milky Way and so is the best laboratory to study in detail the ISM of low metallicity galaxies.

Determinations of oxygen abundances in this work were done with three methods: i) using RLs, ii) using the direct method for CELs, and iii) using CELs relaxing the homogeneous temperature assumption. The first two methods are not compatible. Temperature inhomogeneities of some sort are required to reconcile observations of RLs and CELs. The ADF only becomes a problem if one demands a homogeneous thermal structure from the start. Our results confirm that the ADF problem can be solved by taking into account the presence of thermal inhomogeneities in a chemically homogeneous medium.

Abundances of H II regions are used to constrain models of many areas of astrophysics, therefore, we need to derive abundances from gaseous nebulae with the highest precision possible. A crucial aspect of the available observations is that they require a complex thermal structure; consequently, thermal inhomogeneities must be taken into account to determine abundances.

There are many ways to obtain a t^2 value (Peimbert & Peimbert 2011), the most commonly used is based on the comparison of abundances derived with [O III] lines with abundances derived using O II lines. In this paper we also obtained t^2 values from He I lines and from the comparison of abundances derived using IUE UV C III] and [C III] lines with abundances derived from optical C II lines. For both NGC 456 and NGC 460, we combined t^2 values of O^{++} and He$^+$ to obtain an average t^2. The t^2 value for C^{++} in NGC 456 was not included in such average of t^2 because optical and UV observations do not come from the same place in the H II region; nonetheless, this t^2(C^{++}) is relevant because it is not consistent with a homogeneous temperature structure in the H II region.

To obtain accurate values of t^2, good S/N is required for the faint lines of He I, C II, and O II. He I and O II for the same volume are consistent within the errors. Since each t^2 value comes from a different element and they have different formation histories, this

is evidence that the material within the nebula is well mixed; otherwise those t^2 values of different elements would differ from one another.

The homogeneous temperature assumption of the direct method should only be taken as a first approximation because, in addition to photoionization, other energy sources have to be taken into account. Temperature inhomogeneities measure the overall importance of the many mechanisms that inject energy into the system. We find that O/H abundances of low metallicity H II regions are systematically underestimated and have to be corrected by a factor of 0.25 - 0.45 dex. We suggest that, if no additional information is available, an increase of 0.35 dex on the O/H ratio should be used; this correction includes temperature inhomogeneities and oxygen depletion into dust.

REFERENCES

Asplund, M., Grevesse, N., Sauval, A. J., & Scott, P. 2009, ARA&A, 47, 481

Bastin, R. J. & Storey, P. J. 2006, in IAU Symp., 234, Planetary Nebulae in Our Galaxy and Beyond, Ed. Barlow, M. J. & Mendez, R. H. (Cambridge: Cambridge Univ. Press), 369

Benjamin, R. A., Skillman, E. D., & Smits, D. P. 1999, ApJ, 514, 307

Benjamin, R. A., Skillman, E. D., & Smits, D. P. 2002, ApJ, 569, 288

Bensby, T. & Feltzing, S. 2006, MNRAS, 367, 1181

Bhatia, A. K. & Kastner, S. O. 1995, ApJS, 96, 325

Bonatto, C., Bica, E., & Alloin, D. 1995, A&A, 112, 78

Bordalo, V. & Telles, E. 2011, ApJ, 735, 52

Butler, K. & Zeippen, C. J. 1989, A&A, 208, 337

Butler, K. & Zeippen, C. J. 1994, A&AS, 108, 1

Caplan, J., Ye, T., Deharveng, L., Turtle, A. J., & Kennicutt, R. C. 1996, A&A, 307, 403

Carigi, L., Coln, P., & Peimbert, M. 2006, ApJ, 644, 924

Carigi, L. & Peimbert, M. 2011, RevMexAA, 47, 139

Davey, A. R., Storey, P. J., & Kisielius, R. 2000, A&AS, 142, 85

Dopita, M. A., Mason, D. J., & Robb, W. D. 1976, ApJ, 207, 102

Dufour, R. J., Shields, G. A., & Talbot, R. J. 1982, ApJ, 252, 461

Ercolano, B., Bastian, N., & Stasińska, G. 2007, MNRAS, 379, 945

Esteban, C., Bresolin, F., Peimbert, M., García-Rojas, J., Peimbert, A., & Mesa-Delgado,
    A. 2009, ApJ, 700, 654

Esteban, C., García-Rojas, J., Peimbert, M., Peimbert, A., Ruíz, M. T., Rodríguez, M., &
    Carigi, L. 2005, ApJ, 618, L95

Esteban, C., Peimbert, M., García-Rojas, J., Ruíz, M. T., Peimbert, A., & Rodríguez, M.
    2004, MNRAS, 355, 229

Esteban, C., Peimbert, M., Torres-Peimbert, S., & Escalante, V. 1998, MNRAS, 295, 401

Galavis M. E., Mendoza C., & Zeippen C. J., 1995, A&AS 111, 347

García-Rojas, J., Esteban, C., Peimbert, M., Rodríguez, M., Ruíz, M. T., & Peimbert, A.
    2004, ApJS, 153, 501

García-Rojas, J. & Esteban, C. 2007, ApJ, 670, 457

Garnett, D. R. 1989, ApJ, 345, 282

Garnett, D. R., Skillman, E. D., Dufour, R. J., Peimbert, M., Torres-Peimbert, S., Terlevich,
    R. J., Terlevich, E., & Shields, G. A. 1995, ApJ, 443, 64

González-Delgado, R. M., Leitherer, C., & Heckman, T. M. 1999, ApJS, 125, 489

Guseva, N. G., Izotov, Y. I., Stasińska, G., Fricke, K. J., Henkel, C., & Papaderos, P. 2011,
    A&A, 529, A149

Hamuy, M., Suntzeff, N. B., Heathcote, S. R., Walker, A. R., Gigoux, P., & Phillips, M. M.
    1994, PASP, 106, 566

Hamuy, M., Walker, A. R., Suntzeff, N. B., Gigoux, P., Heathcote, S. R., & Phillips, M. M. 1992, PASP, 104, 533

Hunter, I., Dufton, P. L., Ryans, R. S. I., Lennon, D. J.; Rolleston, W. R. J., Hubeny, I., & Lanz, T. 2005, A&A, 436, 687

Izotov, Y. I. 2010, in IAU Symp., 268, Light Elements in the Universe, Ed. Charbonnel, C., Tosi, M., Primas, F. & Chiappini, C., 107

Kaufman, V. & Sugar, J. 1986, JPCRD, 15, 321

Keenan, F. P., Hibbert, A., Ojha, P. C., & Caylon, E. S. 1993, Phys. Scr., 48, 129

Kewley, L. & Ellison, S. 2008, ApJ, 681, 1183

Kingdon, J., & Ferland, G. 1995, ApJ, 442, 714

Lennon, D. J. & Burke, V. M. 1994, A&AS, 103, 273

Liu, X., Shapley, A. E., Coil, A. L., & Ma, C.-P. 2008, ApJ, 678, 758

Liu, X.-W., Storey, P. J., Barlow, M. J., Danziger, I. J., Cohen, M., & Bryce, M. 2000, MNRAS, 312, 585

McLaughlin, B. M. & Bell, K. L. 1993, ApJ, 408, 753

Mannucci, F., Cresci, G., Maiolino, R., Marconi, A., & Gnerucci, A. 2010, MNRAS, 408, 2115

Mesa-Delgado, A., Esteban, C., García-Rojas, J., Luridiana, V., Bautista, M., Rodríguez, M., López-Martín, L., & Peimbert, M. 2009, MNRAS, 395, 855

Mesa-Delgado, A., López-Martín, L., Esteban, C., García-Rojas, J., & Luridiana, V. 2009, MNRAS, 394, 693

Montenegro, A., Eby, M., Kaplan, J. O., Meissner, K. J., & Weaver, A. J. 2006, GeoRL, 33, L08703

O'Dell, C. R., Peimbert, M., & Peimbert, A. 2003, AJ, 125, 2590

Pagel, B. E. J., Edmunds, M. G., Fosbury, R. A. E., & Webster, B. L. 1978, MNRAS, 184, 569

Peimbert, A. 2003, ApJ, 584, 735

Peimbert, A., & Peimbert, M. 2010, ApJ, 724, 791

Peimbert, A., Peimbert, M., & Luridiana, V. 2002, ApJ, 565, 668

Peimbert, A., Peimbert, M., & Ruíz, M. T. 2005, ApJ, 634, 1056

Peimbert, A., Peña-Guerrero, M. A., & Peimbert, M. 2011, (in preparation)

Peimbert, M. 1967, ApJ, 150, 825

Peimbert, M., & Costero, R. 1969, Bol. Obs. Tonantzintla y Tacubaya, 5, 3

Peimbert, M., & Peimbert, A. 2006, in IAU Symp., 234, Planetary Nebulae in our Galaxy and Beyond, Ed. Barlow, M. J. & Méndez, R. H. (Cambridge: Cambridge University Press), 227

Peimbert, M., & Peimbert, A. 2011, RevMexAA (Serie de Conferencias), 39, 1

Peimbert, M., Peimbert, A., Carigi, L., & Luridiana, V. 2010, in IAU Symp., 268, Light Elements in the Universe, Ed. Charbonnel, C., Tosi, M., Primas, F. & Chiappini, C., 91

Peimbert, M., Peimbert, A., Esteban, C., García-Rojas, J., Bresolin, F., Carigi, L., Ruíz, M. T., & López-Sánchez, A. R. 2007, RevMexAA (Serie de Conferencias), 29, 72

Peimbert, M., Peimbert, A., & Ruiz, M. T. 2000, ApJ, 541, 688

Peimbert, M., Peimbert, A., Ruiz, M. T., & Esteban, C. 2004, ApJS, 150, 431

Peimbert, M., Storey, P. J., & Torres-Peimbert, S. 1993, ApJ, 414, 626

Peimbert, M. & Torres-Peimbert, S. 1976, ApJ, 203, 581

Peimbert, M., Torres-Peimbert, S., & Luridiana, V. 1995, RevMexAA, 31, 131

Pérez-Montero, E., García-Benito, R., Díaz, Á. I., Pérez, E., & Kehrig, C. 2008, ASPCS, 396, 285

Pilyugin, L., Thuan, T. X., & Vílchez, J. M. 2007, MNRAS, 376, 353

Porter, R. L., Ferland, G. J., & MacAdam, K. B. 2007, ApJ, 657, 327

Pradhan, A. K., Montenegro, M., Nahar, S. N., & Eissner, W. 2006, MNRAS, 366, 6

Przybilla, N., Nieva, M. F., & Butler, K. 2008, ApJ, 688, L103

Ramsbottom, C. A., Bell, K. L., & Stafford, R. P. 1996, ADNDT, 63, 57

Relaňo, M., Peimbert, M., & Beckman, J. 2002, ApJ, 564, 704

Rolleston, W. R. J., Venn, K., Tolstoy, E., & Dufton, P. L. 2003, A&A, 400, 21

Ruíz, M. T., Peimbert, A., Peimbert, M., & Esteban, C. 2003, ApJ, 595, 247

Sawey, P. M. J. & Berrington, K. A., 1993, Atomic Data and Nuclear Data Tables, 55, 81

Seaton, M. J. 1979, MNRAS, 187, 73

Simón-Díaz, S. & Stasińska, G. 2011, A&A, 526, A48

Stasińska, G., Tenorio-Tagle, G. Rodríguez, M., & Henney, W. J. 2007, A&A, 471, 193

Storey, P. J. 1994, A&A, 282, 999

Storey, P. J. & Hummer, D. G. 1995, MNRAS, 272, 41

Tayal, S. S. 2007, ApJ, 171, 331

Tenorio-Tagle, G. 1996, A. J. 111, 1641

Thuan, T. X., Pilyugin, L., S., & Zinchenko, I. A. 2010, ApJ, 712, 1029

Torres-Peimbert, S., Peimbert, M., & Peña, M. 1990, A&A, 233, 540

Tremonti, C. A., Heckman, T. M., Kauffmann, G., Brinchmann, J., Charlot, S., White, S. D. M., Seibert, M., Peng, E. W., Schlegel, D. J., Uomoto, A., Fukugita, M., & Brinkmann, J. 2004, ApJ, 613, 898

Tsamis, Y. G., Barlow, M. J., Liu, X.-W., Dazinger, I. J., Storey, P. J. 2003, MNRAS, 338, 687

Tsamis, Y. G., Barlow, M. J., Liu, X.-W., Storey, P. J., & Danziger, I. J. 2004, MNRAS, 353, 953

Tsamis, Y. G. & Péquignot, D. 2005, MNRAS, 364, 687

Tsamis, Y. G. & Walsh. 2011, MNRAS, doi: 10.1111/j.1365-2966.2011.19396.x

Tsamis, Y., Walsh, J. R., Vílchez, J. M., & Péquignot, D. 2011, MNRAS, 412, 1367

Venn, K. A. 1999, ApJ, 518, 405

Venn, K. A., Lennon, D. J., Kaufer, A., McCarthy, J. K., Przybilla, N., Kudritzki, R. P., Lemke, M., Skillman, E. D. & Smartt, S. J. 2001, ApJ, 547, 765

Vila-Costas, M. B. & Edmunds, M. G. 1992, MNRAS, 259, 121

Wang, W., Liu, X.-W., Zhang, Y., & Barlow, M. J. 2004, A&A, 427, 873

Westerlund, B. E. 1990, A&A Rev., 2, 29

Wiese, W. L., Fuhr, J. R., & Deters, T. M. 1996, JPCRD, Monograph 7

Zaritsky, D., Kennicutt, R. C., Jr. & Huchra, J. P. 1994, ApJ, 420, 87

Zeippen, C. J., Butler, K., & Le Bourlot, J. 1987, A&A, 188, 251

Table 1.   Journal of Observations

Grism	Filter	λ (Å)	Resolution ($\lambda/\Delta\lambda$)	Exp. Time (s)
GRIS-600B+12	-	3450–5900	1300	3×720
GRIS-600R+14	GG435	5250–7450	1700	3×600
GRIS-300V	GG375	3850–8800	700	3×120

Table 2.   Absolute Equivalent Widths

Hydrogen		Helium	
Line	$\frac{\text{EW}_{\text{abs}}(\text{Line})}{\text{EW}_{\text{abs}}(\text{H}\beta)}$	Line	$\frac{\text{EW}_{\text{abs}}(\text{Line})}{\text{EW}_{\text{abs}}(\text{H}\beta)}$
Hα[a]	0.90	3820[a]	0.108
Hγ[a]	1.05	4026[a]	0.100
Hδ[a]	1.08	4388[a]	0.084
H7[a]	0.99	4471[a]	0.179
H8[a,b]	0.93	4922[a]	0.107
H9[a]	0.78	4009[d]	0.100
H10[c]	0.67	5016[d]	0.114
H11[c]	0.54	5048[d]	0.115
H12[c]	0.42	5876[d]	0.138
H13[c]	0.35	6678[d]	0.082
H14[c]	0.30	7281[d]	0.032
H15[c]	0.25		
H16[c]	0.20		
H17[c]	0.16		
H18[c]	0.13		
H19[c]	0.10		
H20[c]	0.08		
H21[c]	0.06		
H22[c]	0.05		

[a]González-Delgado et al. (1999).

[b]Note that He I(3889) is included with H8.

[c]Extrapolations based on VLT echelle observations of 30 Doradus (Peimbert 2003).

[d]M. Cerviño, private conversation.

Table 3.   NCG 456: Line Intensities for Positions 1, 2, and 3

			Position 1			Position 2			Position 3		
λ (Å)	Id.	$f(\lambda)$	$F(\lambda)$	$I(\lambda)$	% err.	$F(\lambda)$	$I(\lambda)$	% err.	$F(\lambda)$	$I(\lambda)$	% err.
3587	He I	0.272	0.56	0.64	18	0.59	0.66	10	0.93	1.02	28
3614	He I	0.271	0.95	1.08	14	1.09	1.22	7	0.91	0.99	29
3634	He I	0.270	0.89	1.01	15	1.23	1.37	7	$\cdots$	$\cdots$	$\cdots$
3676	H 22	0.269	$\cdots$	$\cdots$	$\cdots$	0.35	0.40	13	$\cdots$	$\cdots$	$\cdots$
3679	H 21	0.268	$\cdots$	$\cdots$	$\cdots$	0.43	0.48	11	$\cdots$	$\cdots$	$\cdots$
3683	H 20	0.267	$\cdots$	$\cdots$	$\cdots$	0.38	0.43	12	0.68	0.76	33
3687	H 19	0.266	$\cdots$	$\cdots$	$\cdots$	0.54	0.61	10	0.64	0.72	34
3692	H 18	0.265	$\cdots$	$\cdots$	$\cdots$	0.63	0.71	9	0.55	0.62	37
3695	H 17	0.264	$\cdots$	$\cdots$	$\cdots$	0.76	0.99	9	0.99	1.35	28
3704	H 16	0.262	$\cdots$	$\cdots$	$\cdots$	1.24	1.56	7	1.18	1.62	25
3712	H 15	0.260	$\cdots$	$\cdots$	$\cdots$	1.22	1.58	7	1.55	2.11	22
3722	H 14+[S III]	0.257	1.54	1.99	11	1.60	2.05	6	1.46	2.11	23
3726	[O II]	0.256	65.02	73.16	2	58.79	65.23	1	61.13	66.59	4
3729	[O II]	0.255	86.89	97.72	2	73.92	81.98	1	83.15	90.54	3
3734	H 13	0.254	2.13	2.69	9	1.70	2.20	6	1.69	2.44	21
3750	H 12	0.250	2.38	3.00	9	2.48	3.11	5	2.09	2.97	19
3770	H 11	0.245	3.14	3.97	8	3.24	4.06	4	3.05	4.20	16
3798	H 10	0.238	4.11	5.14	7	4.31	5.34	4	3.95	5.39	14
3820	He I	0.233	0.75	0.92	16	0.80	0.97	8	1.65	1.91	21
3836	H 9	0.229	5.97	7.29	6	5.98	7.26	3	5.48	7.19	12
3867	[Ne III]	0.222	17.91	19.82	3	22.23	24.30	2	22.82	24.55	6
3889	H 8+He I	0.218	16.71	19.25	3	16.57	18.93	2	17.26	20.04	7
3967	[Ne III]	0.201	20.25	22.68	3	22.15	24.01	2	21.25	22.68	6
4009	He I	0.193	$\cdots$	$\cdots$	$\cdots$	0.17	0.69	18	$\cdots$	$\cdots$	$\cdots$
4026	He I	0.190	1.37	1.58	12	1.60	1.90	6	1.71	1.97	21
4067	[S II]	0.182	1.01	1.10	14	0.93	0.99	8	0.71	0.76	33
4076	[S II]	0.181	0.32	0.35	24	0.30	0.32	14	$\cdots$	$\cdots$	$\cdots$
4102	Hδ	0.176	23.81	26.65	3	23.82	26.45	2	23.62	26.53	6
4125	[Fe II]	0.172	$\cdots$	$\cdots$	$\cdots$	0.30	0.32	14	$\cdots$	$\cdots$	$\cdots$
4144	He I	0.169	$\cdots$	$\cdots$	$\cdots$	0.30	0.42	14	$\cdots$	$\cdots$	$\cdots$
4169	O II	0.164	$\cdots$	$\cdots$	$\cdots$	0.18	0.19	18	$\cdots$	$\cdots$	$\cdots$
4185	O II	0.161	$\cdots$	$\cdots$	$\cdots$	0.12	0.13	21	$\cdots$	$\cdots$	$\cdots$
4267	C II	0.143	<0.30	<0.30	$\cdots$	0.04	0.04	40	<0.30	<0.30	$\cdots$
4340	Hγ	0.128	45.03	48.25	2	44.52	47.51	1	44.29	47.28	4
4363	[O III]	0.122	4.12	4.34	7	4.36	4.57	4	4.22	4.38	13
4388	He I	0.116	0.58	0.66	18	0.42	0.50	12	$\cdots$	$\cdots$	$\cdots$
4471	He I	0.094	3.77	4.13	7	3.72	3.97	4	3.89	4.20	14
4563	Mg I]	0.070	$\cdots$	$\cdots$	$\cdots$	0.08	0.08	27	$\cdots$	$\cdots$	$\cdots$
4571	Mg I]	0.068	$\cdots$	$\cdots$	$\cdots$	0.05	0.05	33	$\cdots$	$\cdots$	$\cdots$
4639+42	O II	0.051	$\cdots$	$\cdots$	$\cdots$	0.06	0.06	30	$\cdots$	$\cdots$	$\cdots$
4649+51	O II	0.049	$\cdots$	$\cdots$	$\cdots$	0.07	0.07	28	$\cdots$	$\cdots$	$\cdots$
4658	[Fe III]	0.047	0.36	0.36	23	0.29	0.30	14	$\cdots$	$\cdots$	$\cdots$
4701	[Fe III]	0.037	0.10	0.11	43	0.10	0.10	24	$\cdots$	$\cdots$	$\cdots$
4711	[Ar IV]+He I	0.034	0.44	0.53	21	0.50	0.59	11	$\cdots$	$\cdots$	$\cdots$

Table 3—Continued

λ (Å)	Id.	$f(\lambda)$	Position 1			Position 2			Position 3		
			$F(\lambda)$	$I(\lambda)$	% err.	$F(\lambda)$	$I(\lambda)$	% err.	$F(\lambda)$	$I(\lambda)$	% err.
4740	[Ar IV]	0.028	$\cdots$	$\cdots$	$\cdots$	0.06	0.06	31	$\cdots$	$\cdots$	$\cdots$
4755	[Fe III]	0.024	$\cdots$	$\cdots$	$\cdots$	0.07	0.07	29	$\cdots$	$\cdots$	$\cdots$
4861	Hβ	0.000	100.00	100.00	2	100.00	100.00	1	100.00	100.00	3
4881	[Fe III]	-0.004	0.24	0.24	28	0.10	0.10	23	$\cdots$	$\cdots$	$\cdots$
4922	He I	-0.013	1.10	1.14	13	1.03	1.07	7	1.29	1.38	24
4959	[O III]	-0.021	116.26	114.42	2	135.29	133.39	1	127.17	124.85	2
4986	[Fe III]	-0.027	0.60	0.59	18	0.30	0.30	14	$\cdots$	$\cdots$	$\cdots$
5007	[O III]	-0.032	345.85	338.55	1	404.17	396.63	1	375.64	367.27	2
5016	He I	-0.034	2.48	2.49	9	2.44	2.45	5	2.74	2.78	17
5041	S III	-0.040	$\cdots$	$\cdots$	$\cdots$	0.11	0.11	22	0.72	0.70	33
5048	He I	-0.041	0.27	0.32	26	0.20	0.25	17	$\cdots$	$\cdots$	$\cdots$
5056	S III	-0.043	$\cdots$	$\cdots$	$\cdots$	0.08	0.07	27	$\cdots$	$\cdots$	$\cdots$
5192	[Ar III]	-0.072	$\cdots$	$\cdots$	$\cdots$	0.08	0.08	26	$\cdots$	$\cdots$	$\cdots$
5198	[N I]	-0.074	0.21	0.20	30	0.12	0.12	21	$\cdots$	$\cdots$	$\cdots$
5270	[Fe III]	-0.089	0.17	0.17	33	0.16	0.16	19	$\cdots$	$\cdots$	$\cdots$
5517	[Cl III]	-0.140	0.41	0.38	22	0.43	0.41	11	0.46	0.43	41
5537	[Cl III]	-0.144	0.33	0.30	24	0.31	0.29	13	0.35	0.33	47
5755	[N II]	-0.191	0.22	0.20	30	0.15	0.14	19	$\cdots$	$\cdots$	$\cdots$
5876	He I	-0.216	11.76	10.58	4	12.25	11.17	2	11.74	10.82	8
6300	[O I]	-0.285	$\cdots$	$\cdots$	$\cdots$	1.11	0.98	7	1.99	1.77	20
6312	[S III]	-0.286	1.12	1.00	19	2.02	1.78	5	1.12	1.00	26
6364	[O I]	-0.294	$\cdots$	$\cdots$	$\cdots$	0.38	0.33	12	2.96	2.62	16
6371	[S III]	-0.295	$\cdots$	$\cdots$	$\cdots$	0.05	0.05	33	$\cdots$	$\cdots$	$\cdots$
6548	[N II]	-0.320	5.42	4.61	6	2.94	2.55	4	2.68	2.35	17
6563	Hα	-0.322	339.15	288.06	1	330.81	287.11	1	327.01	287.21	2
6583	[N II]	-0.324	12.06	10.83	4	8.19	7.10	3	8.04	7.05	10
6678	He I	-0.337	3.45	2.90	7	3.73	3.23	4	3.81	3.37	14
6716	[S II]	-0.342	12.85	10.83	4	10.04	8.63	2	10.34	9.00	9
6731	[S II]	-0.343	9.46	7.97	5	8.35	7.18	3	7.20	6.26	10
7065	He I	-0.383	2.54	2.11	9	2.95	2.51	4	2.32	2.02	18
7136	[Ar III]	-0.391	8.87	7.30	5	9.90	8.34	2	8.86	7.57	9
7281	He I	-0.406	0.71	0.59	16	0.75	0.63	9	$\cdots$	$\cdots$	$\cdots$
7319	[O II]	-0.410	3.65	2.97	7	3.79	3.16	4	2.87	2.43	16
7330	[O II]	-0.411	2.98	2.43	8	3.03	2.53	4	2.45	2.08	18
7442	N II	-0.422	0.24	0.20	28	0.25	0.21	15	$\cdots$	$\cdots$	$\cdots$
7510	C II	-0.429	0.82	0.67	15	1.06	0.88	7	1.03	0.87	27
7552	[Fe II]	-0.440	0.81	0.65	15	0.88	0.72	8	0.93	0.78	29
7720	[Fe II]	-0.450	0.86	0.68	15	1.14	0.94	7	$\cdots$	$\cdots$	$\cdots$
7751	[Ar III]	-0.452	2.02	1.62	10	2.05	1.68	5	0.99	0.83	28
7994	N II	-0.473	1.35	1.07	12	1.38	1.12	6	$\cdots$	$\cdots$	$\cdots$
8360	P 22	-0.503	$\cdots$	$\cdots$	$\cdots$	0.14	0.12	20	$\cdots$	$\cdots$	$\cdots$
8375	P 21	-0.504	$\cdots$	$\cdots$	$\cdots$	0.11	0.08	23	$\cdots$	$\cdots$	$\cdots$
8413	P 19	-0.507	$\cdots$	$\cdots$	$\cdots$	0.22	0.18	16	$\cdots$	$\cdots$	$\cdots$
8467	P 17	-0.512	$\cdots$	$\cdots$	$\cdots$	0.36	0.29	12	$\cdots$	$\cdots$	$\cdots$

Table 3—Continued

			Position 1			Position 2			Position 3		
λ (Å)	Id.	$f(\lambda)$	$F(\lambda)$	$I(\lambda)$	% err.	$F(\lambda)$	$I(\lambda)$	% err.	$F(\lambda)$	$I(\lambda)$	% err.
8487	[Fe II]	-0.514	$\cdots$	$\cdots$	$\cdots$	1.91	1.53	5	2.60	2.12	17
8502	P 16+[C III]	-0.515	$\cdots$	$\cdots$	$\cdots$	0.51	0.41	10	$\cdots$	$\cdots$	$\cdots$
8546	P 15+[Cl III]	-0.518	0.43	0.33	21	0.45	0.36	11	1.57	1.28	22
8599	P 14	-0.523	0.34	0.26	24	0.58	0.46	10	$\cdots$	$\cdots$	$\cdots$
8665	P 13	-0.528	2.59	1.99	9	0.80	0.64	8	1.43	1.16	23
8694	N II+[Ne II]	-0.530	$\cdots$	$\cdots$	$\cdots$	0.13	0.10	21	$\cdots$	$\cdots$	$\cdots$
8751	P 12	-0.535	$\cdots$	$\cdots$	$\cdots$	1.01	0.80	7	$\cdots$	$\cdots$	$\cdots$
$EW(\mathrm{H}\beta)$, in Å			341			383			227		
$EW_{abs}(\mathrm{H}\beta)$, in Å			2.4±0.1			2.0±0.1			2.0±0.1		
$C(\mathrm{H}\beta)$, in dex			0.16±0.03			0.19±0.03			0.21±0.03		
$F(\mathrm{H}\beta)$, in erg s^{-1} cm^{-2}			1.66×10^{-13}			1.04×10^{-13}			2.46×10^{-14}		
$I(H\beta)$, in erg s^{-1} cm^{-2}			2.71×10^{-13}			1.60×10^{-13}			3.62×10^{-14}		

Table 4.   NCG 460: Line Intensities of Position 1

λ (Å)	Id.	$f(\lambda)$	$F(\lambda)$	$I(\lambda)$	% err.
3695	H 17	0.264	0.84	1.06	20
3704	H 16	0.262	2.03	2.42	13
3712	H 15	0.260	1.68	2.07	14
3722	H 14+[S III]	0.257	2.35	3.05	12
3726	[O II]	0.246	99.14	111.49	2
3729	[O II]	0.255	118.27	132.94	2
3734	H 13	0.254	1.82	2.52	14
3750	H 12	0.250	2.30	2.92	12
3770	H 11	0.245	4.74	5.65	9
3798	H 10	0.238	5.25	6.28	8
3820	He I	0.233	2.66	3.04	11
3836	H 9	0.229	6.29	7.49	7
3867	[Ne III]	0.222	19.41	21.47	4
3889	H 8+He I	0.218	17.53	20.04	5
3967	[Ne III]	0.201	21.89	22.68	4
4026	He I	0.193	2.02	2.11	15
4067	[S II]	0.182	1.92	0.76	23
4102	Hδ	0.176	24.47	26.53	4
4340	Hγ	0.128	45.48	48.77	3
4363	[O III]	0.122	3.43	3.62	10
4471	He I	0.094	3.97	4.27	9
4563	Mg I]	0.070	0.69	0.71	22
4571	Mg I]	0.068	0.31	0.32	33
4861	Hβ	0.000	100.00	100.00	2
4881	[Fe III]	-0.004	0.82	0.82	21
4922	He II	-0.013	1.21	1.28	17
4959	[O III]	-0.021	100.79	99.07	2
5007	[O III]	-0.032	303.60	296.83	1
5016	He I	-0.034	2.28	2.31	12
5876	He I	-0.216	11.50	10.39	6
6300	[O I]	-0.285	2.31	2.00	12
6312	[S III]	-0.286	2.20	1.90	13
6548	[N II]	-0.320	5.32	4.53	8
6563	Hα	-0.322	359.21	305.67	1
6583	[N II]	-0.324	15.00	12.73	5
6678	He I	-0.337	3.81	3.26	10
6716	[S II]	-0.342	27.65	23.26	4
6731	[S II]	-0.343	19.15	16.10	4
7065	He I	-0.383	2.65	2.22	11
7136	[Ar III]	-0.391	9.53	7.83	6
7281	He I	-0.406	1.37	1.14	16
7319	[O II]	-0.410	4.75	3.87	9
7330	[O II]	-0.411	3.85	3.13	10
7751	[Ar III]	-0.452	2.11	1.68	13
EW(Hβ), in Å				285	
EW_{abs}(Hβ), in Å				2.0±0.1	

Table 4—Continued

λ (Å)	Id.	$f(\lambda)$	$F(\lambda)$	$I(\lambda)$	% err.
$C(\mathrm{H}\beta)$, in dex			0.21 ± 0.03		
$F(\mathrm{H}\beta)$, in erg s^{-1} cm^{-2}			3.97×10^{-14}		
$I(H\beta)$, in erg s^{-1} cm^{-2}			6.21×10^{-14}		

Table 5.   Atomic Data for CELs in IRAF v2.15.1

Ion	Transition Probabilities	Collisional Strengths
N^0	Wiese et al. (1996)	Dopita et al. (1976)
N^+	Wiese et al. (1996)	Lennon & Burke (1994)
O^0	Wiese et al. (1996)	Bhatia & Kastner (1995)
O^+	Wiese et al. (1996)	McLaughlin & Bell (1993)
O^{++}	Wiese et al. (1996)	Lennon & Burke (1994)
Ne^{++}	Kaufman & Sugar (1986)	Butler & Zeippen (1994)
S^+	Keenan et al. (1993)	Ramsbottom et al. (1996)
S^{++}	Kaufman & Sugar (1986)	Galavis et al. (1995)
Cl^{++}	Kaufman & Sugar (1986)	Butler & Zeippen (1989)
Ar^{++}	Kaufman & Sugar (1986)	Galavis et al. (1995)
Ar^{+3}	Kaufman & Sugar (1986)	Zeippen et al. (1987)

Table 6.   Densities and Temperatures

| | NGC 456 | | | NGC 460 |
	Position 1	Position 2	Position 3	Position 1
Densities (cm^{-3})				
[O II]	80±15	130±30	60±30	170±20
[S II]	< 250	250±60	< 500	< 150
[Cl III]	< 3000	< 1000	< 1300	$\cdots$
Temperatures (K)				
[O II]	13500±250	12400±400	12600±800	12600±600
[N II]	11300±850	11700±1000	$\cdots$	$\cdots$
[S II]	8500±700	9700±450	7300±1400	8500±450
[O III]	12650±200	12165±160	12300±550	12400±450

Table 7.   Ionic Abundance Determinations from Recombination Lines[a]

Ion	NGC 456					
---	Position 1		Position 2		Position 3	
	$t^2 = 0.000$	$t^2 = 0.035 \pm 0.032$	$t^2 = 0.000$	$t^2 = 0.067 \pm 0.013$	$t^2 = 0.000$	$t^2 = 0.040 \pm 0.040$
He$^+$	10.910±0.011	10.906±0.012	10.923±0.008	10.918±0.008	10.945±0.015	10.924±0.019
C^{++}	$\cdots$	$\cdots$	7.47±0.18	7.46±0.18	$\cdots$	$\cdots$
O^{++}	$\cdots$	$\cdots$	8.20±0.19	8.20±0.19	$\cdots$	$\cdots$

Ion	NGC 460 Position 1	
	$t^2 = 0.000$	$t^2 = 0.036 \pm 0.027$
He$^+$	10.935±0.014	10.921±0.015
O^{++}	7.86±0.30	7.86±0.30

[a]In units of 12+ Log $N(\mathrm{X}^{+i})/N(\mathrm{H})$, gaseous content only.

Table 8.   Ionic Abundance Determinations from Collisionally Excited Lines[a]

Ion	NGC 456					
	Position 1		Position 2		Position 3	
	$t^2 = 0.000$	$t^2 = 0.035 \pm 0.032$	$t^2 = 0.000$	$t^2 = 0.067 \pm 0.013$	$t^2 = 0.000$	$t^2 = 0.040 \pm 0.040$
C^{++}	$\cdots$	$\cdots$	6.75±0.15	7.28±0.18	$\cdots$	$\cdots$
N^0	$\cdots$	$\cdots$	4.54±0.08	4.71±0.06	$\cdots$	$\cdots$
N^+	6.03±0.03	6.15±0.14	5.92±0.04	6.07±0.04	5.90±0.07	6.02±0.16
O^0	$\cdots$	$\cdots$	6.00±0.06	6.15±0.05	6.18±0.11	6.30±0.18
O^+	7.31±0.03	7.46±0.18	7.35±0.05	7.53±0.04	7.38±0.10	7.53±0.19
O^{++}	7.76±0.02	7.87±0.13	7.88±0.01	8.13±0.07	7.83±0.06	7.96±0.17
Ne^{++}	6.96±0.03	7.09±0.14	7.11±0.02	7.39±0.07	7.10±0.07	7.25±0.19
S^+	5.32±0.03	5.44±0.14	5.33±0.03	5.48±0.04	5.29±0.07	5.40±0.15
S^{++}	6.24±0.05	6.37±0.14	6.30±0.03	6.58±0.07	6.03±0.12	6.18±0.22
Cl^{++}	4.34±0.09	4.45±0.18	4.40±0.05	4.64±0.08	4.43±0.16	4.56±0.29
Ar^{++}	5.58±0.03	5.68±0.11	5.64±0.02	5.86±0.06	5.42±0.06	5.54±0.16
Ar^{+3}	$\cdots$	$\cdots$	3.88±0.12	4.14±0.14	$\cdots$	$\cdots$

	NGC 460 Position 1	
	$t^2 = 0.000$	$t^2 = 0.036 \pm 0.027$
N^+	6.16±0.05	6.28±0.12
O^+	7.57±0.06	7.73±0.16
O^{++}	7.72±0.05	7.84±0.12
Ne^{++}	7.03±0.06	7.16±0.14
S^+	5.71±0.04	5.83±0.12
S^{++}	6.30±0.08	6.43±0.14
Ar^{++}	5.62±0.04	5.72±0.11

[a]In units of 12+ Log $N(X^{+i})/N(H)$, gaseous content only.

Table 9.   NGC 456 Position 2 Gaseous Abundance Determinations[a]

Element	This paper		PTP[b]	PEFW[c]	GISFHP[d]
	$t^2 = 0.000$	$t^2 = 0.067 \pm 0.013$	$t^2 = 0.055$	$t^2 = 0.000$	$t^2 = 0.000$
He[e]	10.923±0.008	10.918±0.008	10.898	$\cdots$	$\cdots$
C[e]	7.57 ±0.18	7.56 ±0.18	$\cdots$	$\cdots$	$\cdots$
C[f]	6.85 ±0.10	7.38 ±0.18	$\cdots$	$\cdots$	$\cdots$
N[f]	6.67 ±0.02	6.89 ±0.03	6.61	6.48	6.43±0.02
O[e]	8.29 ±0.19	8.29 ±0.19	$\cdots$	$\cdots$	$\cdots$
O[f]	7.99 ±0.02	8.23 ±0.05	8.12	8.07	8.06±0.01
Ne[f]	7.25 ±0.02	7.51 ±0.05	7.22	7.12	7.22±0.02
S[f]	6.45 ±0.04	6.72 ±0.13	$\cdots$	$\cdots$	6.46±0.02
Cl[f]	4.53 ±0.05	4.78 ±0.11	$\cdots$	$\cdots$	4.66±0.04
Ar[f]	5.76 ±0.04	5.98 ±0.13	$\cdots$	$\cdots$	5.77±0.01

[a]In units of 12+ Log $N(\mathrm{X})/N(\mathrm{H})$.

[b]Peimbert & Torres-Peimbert (1976).

[c]Pagel et al. (1978).

[d]Guseva et al. (2011).

[e]Recombination lines.

[f]Collisionally excited lines.

Table 10.   NGC 456: Positions 1 and 3 Gaseous Abundance Determinations[a]

Element	Position 1		Position 3	
	$t^2 = 0.000$	$t^2 = 0.035 \pm 0.032$	$t^2 = 0.000$	$t^2 = 0.040 \pm 0.040$
He[b]	10.910±0.011	10.906±0.012	10.945±0.015	10.924±0.019
N[c]	6.70 ±0.02	6.79 ±0.07	6.57 ±0.05	6.68 ±0.09
O[c]	7.89 ±0.02	8.01 ±0.10	7.96 ±0.05	8.10 ±0.13
Ne[c]	7.13 ±0.02	7.26 ±0.09	7.26 ±0.05	7.41 ±0.13
S[c]	6.39 ±0.04	6.52 ±0.17	6.20 ±0.07	6.35 ±0.21
Cl[c]	4.39 ±0.03	4.50 ±0.08	4.48 ±0.05	4.61 ±0.08
Ar[c]	5.71 ±0.05	5.81 ±0.16	5.55 ±0.06	5.67 ±0.19

[a]In units of 12+ Log $N(\text{X})/N(\text{H})$.

[b]Recombination lines.

[c]Collisionally excited lines.

Table 11.   NGC 460 Position 1 Gaseous Abundance Determinations[a]

Element	This paper		PEFW[b]
	$t^2 = 0.000$	$t^2 = 0.036 \pm 0.027$	$t^2 = 0.000$
He[c]	10.935±0.014	10.921±0.015	$\cdots$
N[d]	6.60 ±0.04	6.70 ±0.07	$\cdots$
O[c]	8.09 ±0.30	8.10 ±0.30	$\cdots$
O[d]	7.96 ±0.04	8.09 ±0.09	8.07
Ne[d]	7.30 ±0.03	7.45 ±0.08	7.36
S[d]	6.50 ±0.06	6.63 ±0.16	$\cdots$
Ar[d]	5.85 ±0.08	5.95 ±0.14	$\cdots$

[a]In units of 12+ Log $N(\mathrm{X})/N(\mathrm{H})$.

[b]Pagel et al. (1978).

[c]Recombination lines.

[d]Collisionally excited lines.

Table 12.   NGC 456, NGC 6822 V, NGC 346, 30 Doradus, the Orion Nebula, and Protosolar Total Abundances Relative to O[a]

Element	NGC 456[b]	NGC 6822 V[c]	NGC 346[d]	30 Doradus[e]	Orion[f]	Sun[g]
$12 + \log$ He/H	10.918±0.008	10.909±0.011	10.900±0.003	10.928±0.003	10.988±0.003	10.98±0.01
$12 + \log$ O/H	8.33±0.05	8.45±0.06	8.21±0.06	8.62±0.05	8.77±0.03	8.73±0.05
$\log$ C/O	−0.83±0.37	−0.34±0.13	−0.93±0.08	−0.48±0.05	−0.25±0.04	−0.26±0.15
$\log$ N/O	−1.44±0.09	−1.40±0.17	−1.40±0.15	−1.27±0.08	−1.04±0.10	−0.86±0.17
$\log$ Ne/O	−0.82±0.11	−0.82±0.09	−0.89±0.06	−0.79±0.06	−0.72±0.08	−0.76±0.14
$\log$ S/O	−1.51±0.19	−1.65±0.09	−1.65±0.12	−1.63±0.10	−1.55±0.05	−1.57±0.13
$\log$ Cl/O	−3.55±0.17	−3.74±0.10	$\cdots$	−3.70±0.12	−3.44±0.05	$\cdots$
$\log$ Ar/O	−2.35±0.18	−2.39±0.08	−2.39±0.10	−2.36±0.10	−2.15±0.06	−2.29±0.13
$\log$ Fe/O	$\cdots$	−1.44±0.10	−1.47±0.10	$\cdots$	−1.27±0.20	−1.19±0.11

[a]The O and C gaseous abundances have been corrected for the fractions of these elements trapped in dust grains, see text.

[b]Values in this column are relative to O with $t^2 = 0.067 \pm 0.013$.

[c]Nebular abundances, values for $t^2 = 0.076 \pm 0.018$, obtained for NGC 6822,from (Peimbert et al. 2005), with the exception of the Fe/O value that comes from stellar data (Venn et al. 2001).

[d]Dufour et al. (1982); Peimbert et al. (2000); Relaño et al. (2002); Peimbert, Peimbert, & Luridiana (2002), values for $t^2 = 0.022 \pm 0.008$. The Fe/O value comes from stellar data (Venn 1999; Rolleston et al. 2003; Hunter et al. 2005).

[e]Peimbert (2003), values for $t^2 = 0.033 \pm 0.005$.

[f]Esteban et al. (2004), values for $t^2 = 0.022 \pm 0.002$. The O and C abundances have been increased by 0.08 dex and 0.10 dex respectively to take into account the fractions of these elements trapped in dust grains. The Cl abundance has been decreased by 0.13 dex due to an error of +1.00 dex in the determination of the Cl^+/H^+ ratio.

[g]Taken from the protosolar abundances of Asplund et al. (2009).

Table 13.   NGC 456 and NGC 460 Total Abundances Relative to O[a]

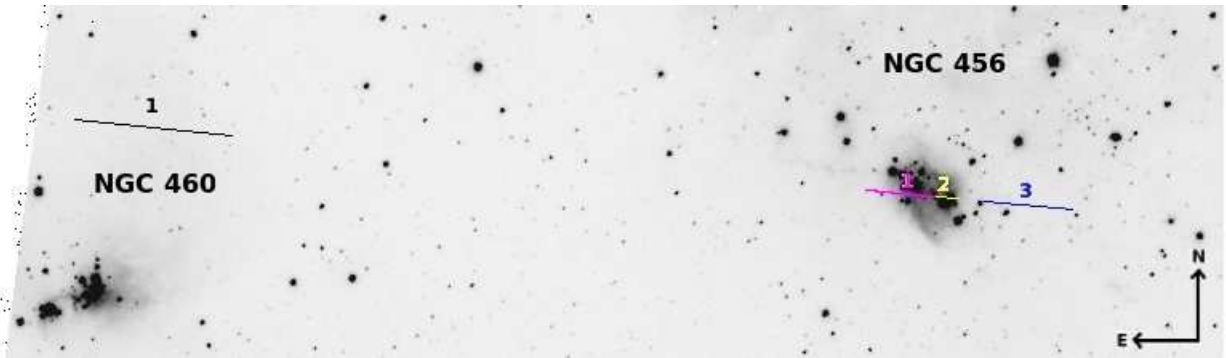| Element	NGC 456 Position 2		NGC 460 Position 1	
	$t^2 = 0.000$	$t^2 = 0.067 \pm 0.013$	$t^2 = 0.000$	$t^2 = 0.036 \pm 0.027$
$12 + \log$ He/H	10.923±0.008	10.918±0.008	10.935±0.014	10.921±0.015
$12 + \log$ O/H	8.09±0.02	8.33±0.05	8.06±0.04	8.19±0.09
$\log$ C/O[b]	−0.82±0.37	−0.83±0.37	$\cdots$	$\cdots$
$\log$ C/O[c]	−1.24±0.12	−0.95±0.23	$\cdots$	$\cdots$
$\log$ N/O	−1.42±0.03	−1.44±0.09	−1.46±0.07	−1.49±0.17
$\log$ Ne/O	−0.83±0.03	−0.82±0.11	−0.76±0.07	−0.74±0.17
$\log$ S/O	−1.64±0.06	−1.51±0.19	−1.56±0.10	−1.56±0.26
$\log$ Cl/O	−3.56±0.06	−3.55±0.17	$\cdots$	$\cdots$
$\log$ Ar/O	−2.32±0.06	−2.35±0.18	−2.20±0.13	−2.24±0.23

[a]The O and C gaseous abundances have been corrected for the fractions of these elements trapped in dust grains, see text.

[b]Abundance from RLs relative to O from RLs.

[c]Abundance from CELs relative to O from CELs.
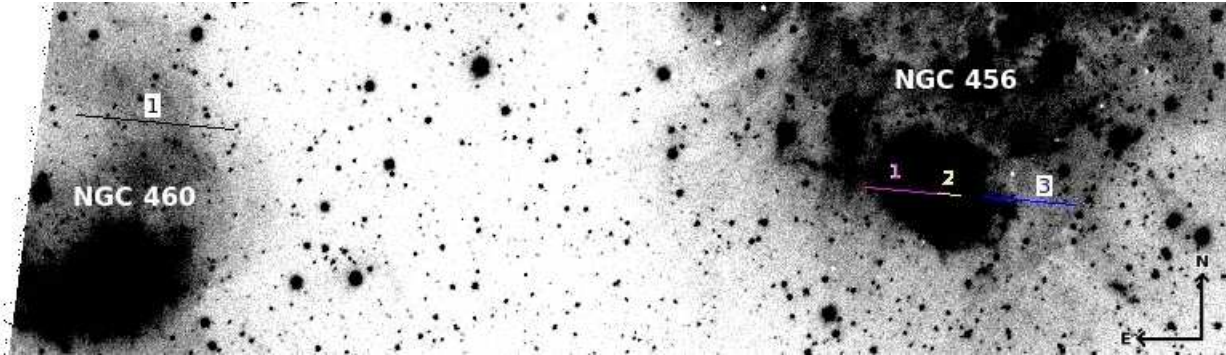
(a)

(b)

Fig. 1.— (1a) VLT image of NGC 460 Position 1 and Positions 1, 2, and 3 of NGC 456. This image of 306" × 87" has Position 2 located at $\alpha = 1^h13^m50.8^s$ and $\delta = -73^o18'03.2''$ (J2000.0), and was taken with a filter that suppresses light bluer than 4350 Å. (1b) Same image but with a different saturation level so that Position 2 in NGC 456 is enhanced.
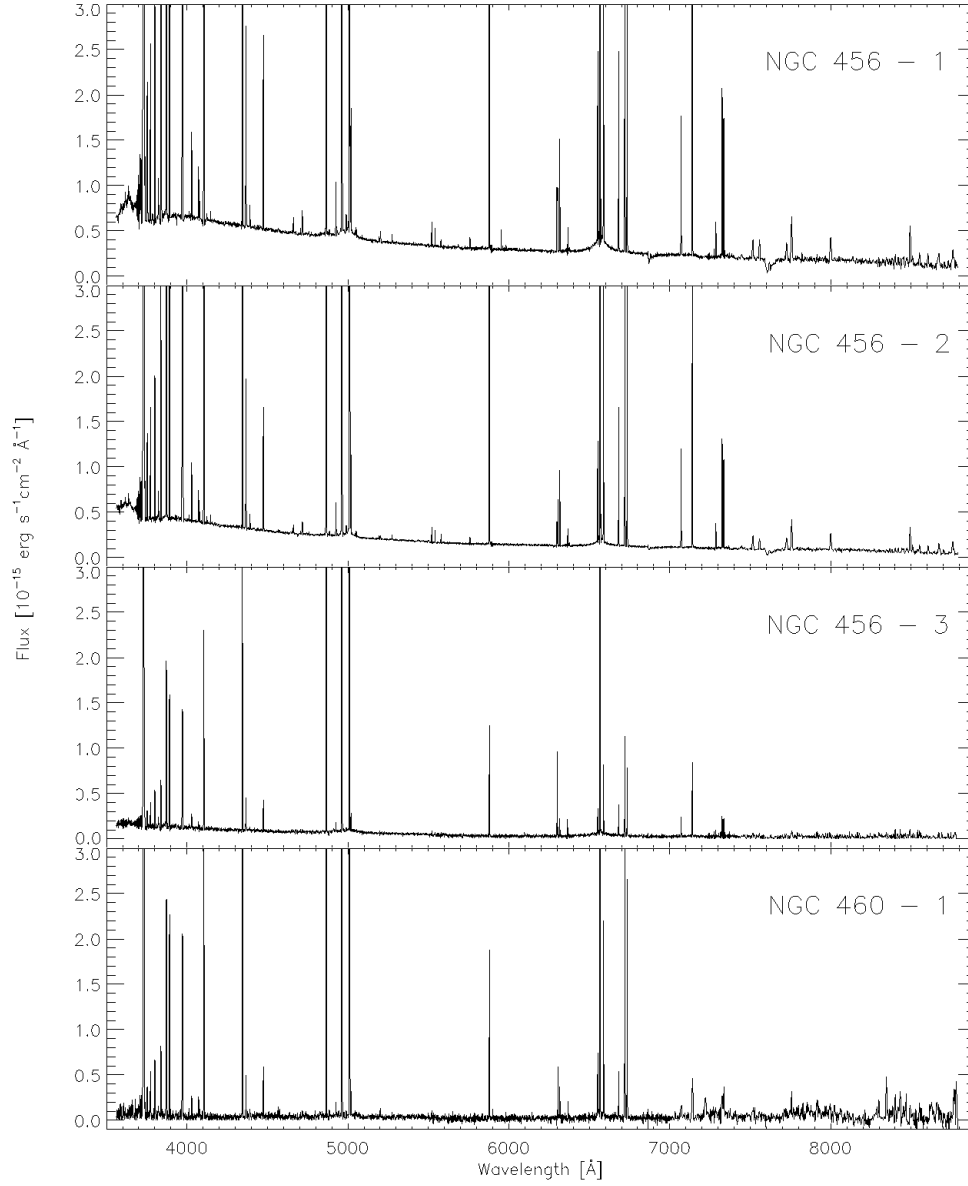
Fig. 2.— Spectra of Positions 1, 2, and 3 in NGC 456, and Position 1 of NGC 460. These spectra include the blue (3600-5500 Å) and red (5500-7400Å) high-resolution spectra, as well as the low-resolution spectrum (7400-8800 Å).
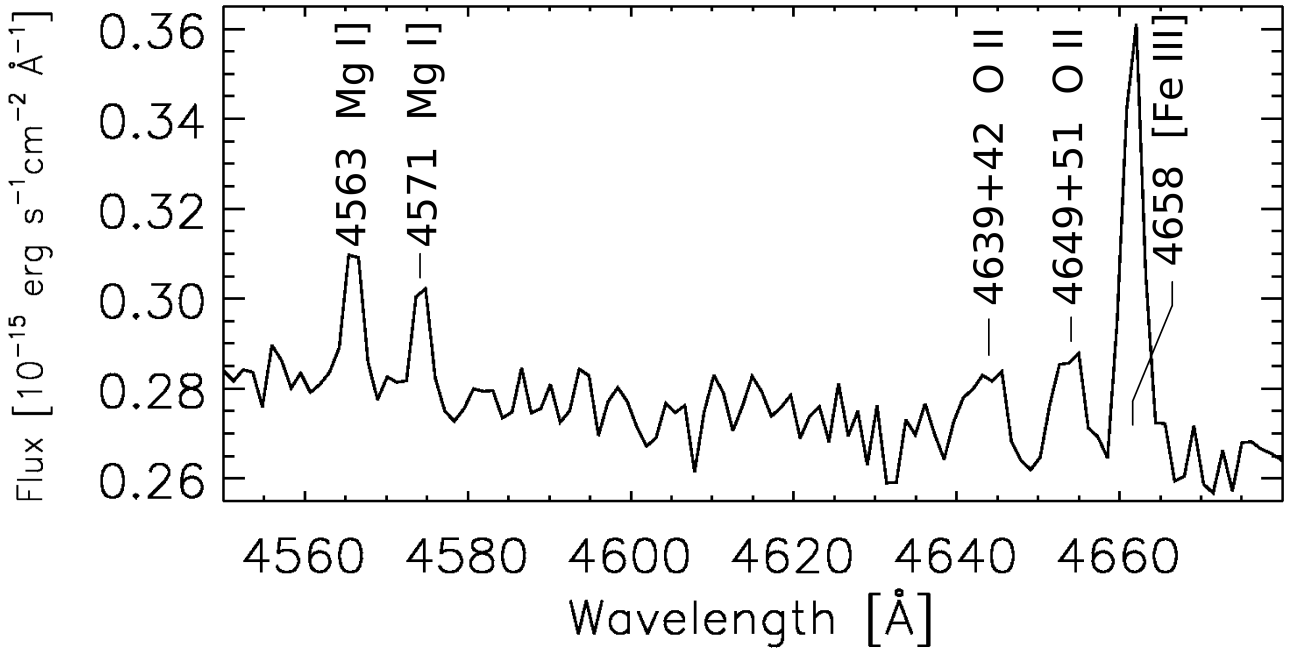
Fig. 3.— Zoom-in of the region between $\lambda4550$ and $\lambda4680$ in NCG 456 Position 2 to show the quality of the data.